Bridge hinge-restrainers built up of NiTi superelastic shape-memory alloys

Filipe P. Amarante dos Santos & Corneliu Cismaşiu

Centro de Investigação em Estruturas e Construção - UNIC, Faculdade de Ciências e Tecnologia, Universidade Nova de Lisboa, Quinta da Torre, 2829-516 Caparica, Portugal

E-mail: fpas@fct.unl.pt

Abstract. This paper analysis the seismic response of a viaduct equipped with a dual superelasic hinge restraining system. The influence of the superelastic restraining area on the structural behaviour of the viaduct is addressed through the analysis of the deck's displacements, velocities and accelerations, for several seismic events. The superelastic restraining system comprises two NiTi pre-strained elements, placed at the abutments of the viaduct. The study is based on a numeric implementation of a rate-dependent constitutive model for shape-memory alloys, calibrated with a set of experimental tensile tests.

Keywords: vibration control, energy dissipation systems, shape- memory alloys, superelasticity, seismic devices, unseating

1. Introduction

Nowadays, it is generally accepted that, for a modern transportation system to be reliable, the design process must ensure an acceptable earthquake risk for all bridge infrastructures. In the case of existing structures, unacceptable seismic safety conditions must be clearly identified and promptly corrected. Designers of bridge retrofit projects have to be able to understand the response of the structural system to potential earthquake ground motions and to design modifications aiming to change undesirable responses of the structure to ones that satisfy the project performance criteria. Past earthquakes have demonstrated that the damage induced in bridges can assume a multitude of different forms, depending, among others, on factors like the ground motion itself, conditions depending on the building site, the adopted bridge structural solution and its specific detailing provisions. Unseating of the bridge superstructure at in-span hinges, or at simple supports, is one of the most severe forms of bridge seismic damage, leading to possible catastrophic consequences. In the case of simply supported bridges, unseating brings about the toppling of the spans from their supports, causing the structure to collapse. This type of failure is either due to shaking or to differential

support movement associated with ground deformation. The problem of unseating is generally associated with inadequate seat lengths or restraint and it is enhanced by skewed, curved, or complex bridge configurations. The unseating mechanism of a multi-framed, simply supported bridge during an earthquake, associated with an in-span hinge, is represented in Figure 1. In order to reduce the seismic response of

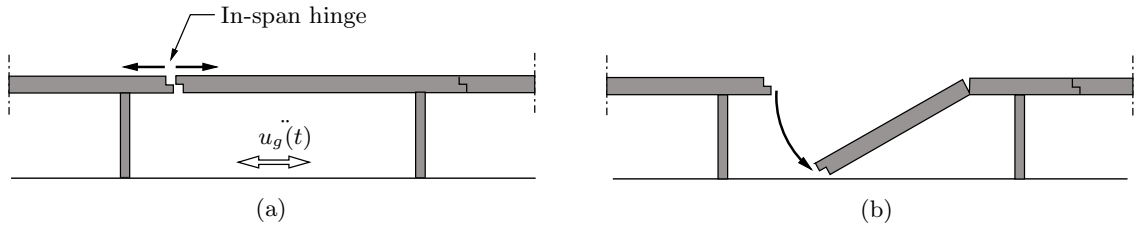

Figure 1. Unseating of bridge at in-span hinge during an earthquake.

bridge structures, they can be provided with special isolating devices called seismic links. According to Eurocode 8 [1], these connection devices may be responsible for the partial or full transmission of the design seismic action, provided that dynamic shock effects are mitigated and taken into account in the design. They are designed to ensure the structural integrity of the bridge and avoid unseating under extreme seismic displacements, while allowing the non-seismic displacements of the bridge to develop without transmitting significant loads. In order to avoid unseating, the code states that new bridges must be provided with appropriate overlap lengths between supporting and supported members at movable connections.

While these new design strategies aim to mitigate the potential unseating problems in new bridges, there are still many existing bridges susceptible to span unseating, due either to the lack of adequate seismic detailing, like the shorter seats usually associated with old constructions, either to potential stronger shaking than the one considered in the original design. These structures require seismic retrofitting in order to modify the seismic response of the bridge, controlling the deck displacements and preventing the unseating of spans. In the case of retrofitting existing bridges, connections implemented by seismic links may be used as an alternative to the provision of the minimum overlap length. Seismic links may also be used between adjacent sections of the deck, at intermediate separation joints, located within the spans. In this case, according to Eurocode 8 [1], the linkage elements may be designed for an action equal to $1.5\,\alpha_g\,S\,M_d$, where α_g is the design ground acceleration on type A ground, S is the soil factor and M_d is the mass of the section of the deck linked to a pier or abutment, or the least of the masses of the two deck sections on either side of the intermediate separation joint.

The traditional approach for this type of restraining systems usually relies on the use of steel cables, which, if designed to remain elastic, lack the ability to dissipate energy and are responsible for the transmission of large seismic forces to other structural components. After yielding, these elements tend to accumulate plastic deformations in repeated loading cycles that can also result in unseating [2]. Several other devices have

been presented in the past decades as unseating prevention devices for bridges, namely in the form of fluid-viscous dampers and metallic dampers [3]. Although theses devices are able to dissipate energy, they lack the capacity for re-centring, which is a very important asset in order to control hinge opening in bridges during seismic actions. The installation of external hinge extenders prevents the supported section of the superstructure from dropping off from its support but has no effect on controlling the deck displacements, which may lead to structural damage in other important components.

To overcome the limitations presented by these devices, and taking advantage of the recent advances in Material Sciences, an alternative solution for seismic retrofitting of structures has been proposed, based on the so called smart materials [2]. Among them, the shape-memory alloys (SMAs), a unique class of metallic alloys exhibiting a peculiar thermo-mechanical property, called superelasticity (SE). This property enables the material to withstand large cyclic deformations (up to 8%), without residual strains, while developing a hysteretic loop, which translates into the ability of the material to dissipate energy. SMAs based seismic damping devices are aimed to concentrate energy dissipation in controlled locations, by taking advantage of the superelastic effect. The high inherent damping exhibited by these alloys, combined with repeatable re-centring capabilities and relatively high strength properties, encouraged the research community to progressively introduce the SMAs in new technological applications related with energy dissipation in Civil Engineering structural design. Several authors have studied the retrofit and rehabilitation of bridges using SMA restraining cables [2, 4, 5, 6, 7], confirming their efficacy when used as seismic links. Analytical models showed that the SMA restrainers reduce relative hinge displacements at the abutment much more effectively than conventional steel cable restrainers [5, 6, 7].

The main objective of this paper is to study the influence of the total cross-section of the SE restraining solution in the seismic response of a bridge. To perform this analysis, a numerical framework has been developed and a rate-dependent constitutive model have been implemented and calibrated with a set of experimental tensile tests.

2. Constitutive model

In a typical SMA constitutive model, the mechanical law relates stress σ, strain ε, temperature T and martensite fraction ξ. Martensite fraction is an internal state variable that represents the extent of the transformation in the material and can be regarded as the fraction of the produced phase. The transformed phase fraction is considered to be in series with the elastic fraction of the response. Several approaches for the mathematical modelling of this elastic component exist in the literature [8]. Among them, the Voight model [9] used in the present paper contemplates two different crystallographic phases, austenite and martensite, not distinguishing between the twinned and the detwinned martensite. It considers a parallel distribution of austenite and martensite within the material and the corresponding Young's modulus is calculated by a rule of mixtures from the values of the pure austenite phase modulus E_A, and the pure martensite phase

modulus E_M, yielding the following mechanical law,

$$\sigma = [\xi E_M + (1-\xi)E_A](\varepsilon - \varepsilon_L \xi) + \theta(T - T_0) \tag{1}$$

where θ is the thermal coefficient of expansion, ε_L the maximum residual strain and T_0 is the temperature at which the thermal strain is defined to be zero [10].

In order to complete the constitutive model, the mechanical law (1) is coupled with the transformation kinetic equations which describe the evolution of the martensite fraction with stress and temperature. Exponential kinetic relations, based on the Magee's transformation kinetics equations [11], are used in the present paper, yielding,

$$\xi^{AM} = 1 - \exp\left[a_M(M_s - T) + b_M\sigma\right], \quad \text{with} \quad \sigma > C_M(T - M_s) \tag{2}$$

for the forward transformation, M_s being the temperature at which the transformation starts in the stress-free state, and

$$\xi^{MA} = \exp[a_A(A_s - T) + b_A\sigma], \quad \text{with} \quad \sigma \leq C_A(T - A_s) \tag{3}$$

for the inverse transformation, where A_s is the temperature at which the transformation starts in the stress-free state. The temperatures at which the forward and inverse transformations end are defined as M_f and A_f, respectively. The exponential law equations (2) and (3) are well known and widely used in the literature [12], once identified the material constants C_M, C_A, a_M, b_M, a_A and b_A [13, 14].

When quasi-static loading conditions are present, the heat exchanges between the SE material and its surrounding environment generates almost isothermic processes. However, as the rate of the dynamic loading increases, the total amount of generated energy per unit time increases accordingly. For fast dynamic cycling, since the dissipation capacity of the thermo-mechanical system is limited by the heat convection mechanism, the generated and the dissipated energy become unbalanced, causing changes in the specimen's temperature and shape of its hysteretic loop. For a SMA constitutive model to conveniently apprehend this phenomena, it is necessary to couple, together with the mechanical and kinetic transformation laws, an adequate heat balance equation [12]. The heat transfer system consists of a cylindrical wire with circular cross section, fixed at both extremities and surrounded by air, at temperature T_f. There are internal energy sources, within the wire, deriving from the enthalpy of the martensitic transformations and internal friction, both occurring during a hysteretic superelastic cycle. Assuming negligible the heat conduction through the wire's extremities, the energy equation may be expressed [15] as,

$$-\rho c V \frac{\mathrm{d}T}{\mathrm{d}t} = \overline{h} A \left[T - T_f\right] - q_{gen} V \qquad \text{with } T(0) = T_f \tag{4}$$

In the above equation, ρ is the density of the material, c the specific heat, V the volume of the sample, A the interface surface and $\overline{h}$ the mean convection coefficient. The power generated per unit volume, q_{gen}, is defined [12] as,

$$q_{gen} = c_L \rho \frac{\mathrm{d}\xi}{\mathrm{d}t} + \frac{\mathrm{d}W}{\mathrm{d}t} \tag{5}$$

The first term is related to the martensite fraction, assuming constant latent heat of transformation, c_L, and the second term to internal friction. In a complete tensile loading-unloading cycle, the dissipated energy by internal friction corresponds to the total area enclosed by the hysteretic cycle. The total generated power during this cycle may, therefore, be computed by dividing the dissipated energy by the duration of the cycle.

3. Assessment of the constitutive model

In order to assess its performances, the model is used to simulate experimental superelastic hysteretic cycles, obtained in classical uniaxial tensile tests. A Zwick/Roell Z050 testing machine is used to test a NiTi SE508 wire ($\phi = 2.40$ mm), with four different strain rates, $\dot{\varepsilon} = 0.008$, 0.067, 0.250 and 0.333%/s. The tests are performed at room temperature ($T_f \simeq 20°$C) and the temperature of the SE wire is continuously monitored with a T-type thermocouple placed at the mid-section of the wire. The material properties used for the corresponding numerical simulations are presented in Table 1.

$E_A = 35000$ MPa	$E_M = 20000$ MPa	$M_f = -45°$ C
$M_s = -35°$ C	$A_s = -15°$ C	$A_f = -5°$ C
$C_M = 6.5$ MPaK^{-1}	$C_A = 6.5$ MPaK^{-1}	$e_L = 3.0\%$
$\rho = 6500$ kg m^{-3}	$c_L = 12914$ J kg^{-1}	$c = 500$ J kg^{-1}K^{-1}
$\overline{h} = 35$ W m^{-2} K^{-1}	$\theta = 0.55$ MPaK^{-1}	

Table 1. Parameters for the numerical simulation of the tensile tests.

The graphs in Figure 2 show the simulated temperature time-history and the corresponding stress-strain diagrams for the quasi-static and dynamic situations, against the experimental values. One can see that the implemented numerical model yields a set of very satisfying results, both for the temperature time-histories and the corresponding stress-strain diagrams. As the strain-rate of the dynamic loading increases from 0.008 to $0.333\%/s$, the amplitude of the temperature variation during the SE cycle increases, in accordance with the experimental results. In what concerns the stress-strain diagrams, for increasing strain-rates, the general shape of the hysteretic loops tends to be steeper and narrower, in conformity with the trend observed in the experimental results.

4. Seismic simulation of NiTi superelastic restrainer cables in a viaduct

The effect of a SMA-based passive control device on the seismic response of a railway viaduct is simulated next. The control device consists in two pre-strained NiTi superelastic wires working in phase opposition [16].

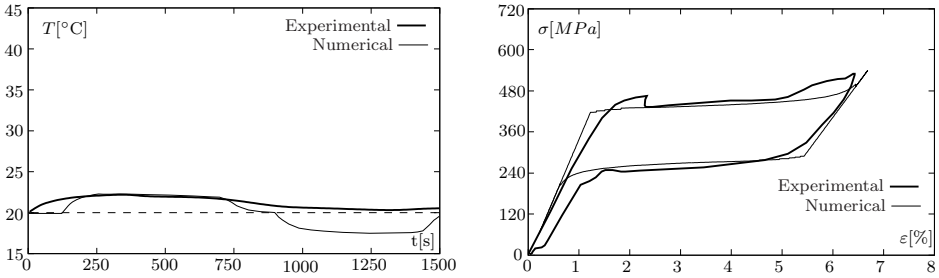

(a) Temperature time-history for $\dot{\varepsilon} = 0.008\%/s$ (b) Stress-strain diagram for $\dot{\varepsilon} = 0.008\%/s$

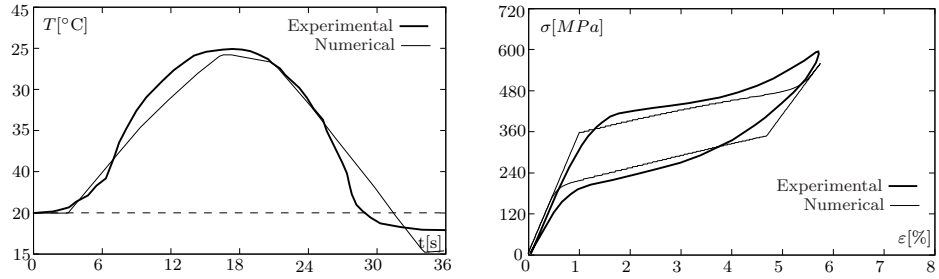

(c) Temperature time-history for $\dot{\varepsilon} = 0.333\%/s$ (d) Stress-strain diagram for $\dot{\varepsilon} = 0.333\%/s$

Figure 2. Numerical model vs. experimental data at temperature $T_f = 20°C$, for increasing strain-rate ($\dot{\varepsilon}$).

A common way to enhance the dissipation capacity of such devices is to pre-strain the SE wires [16, 17, 18]. The influence of the pre-strain is illustrated in Figure 3, representing stress-strain diagrams resulting from a quasi-static harmonic cycle, yielding the full extent of the martensitic transformation in the wires. The system with no

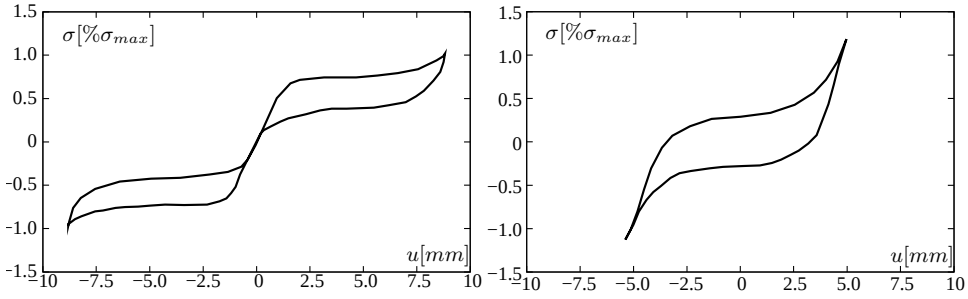

(a) Pre-strain = 0 (d) Pre-strain = 2.0%

Figure 3. Effect of the pre-strain in two SE wires working in phase opposition.

pre-stress yields the stress-strain diagram indicated in Figure 3(a), presenting the development of a full tension/compression SE hysteresis with an equivalent viscous damping of about 10%. When a 2% pre-strain is introduced in the wires, the equivalent viscous damping increases to 23%, as the hysteresis changes from two distinct SE areas to a single hysteretic curve, as illustrated in Figure 3(b).

The structure used for the seismic simulation is the São Martinho railway

viaduct [16]. This viaduct is a pre-stressed concrete railway viaduct with a total length, between abutments, of 852.0 m. It is built up of seven, 113.6 m length, independent segments and one segment of 56.8 m, adjacent to the south abutment. These segments are divided into 28.4 m spans and are structurally independent. The railway deck is a 13.0 m wide beam slab, comprising two 2.0×1.4 m main girders. The foundations are materialised by ϕ1.2 m piles with an average length of about 30.0 m. The concrete piers are tubular and have an average height of 12.0 m. Each pier is supported by five piles. A simplified numerical model of one of these segments is combined with a SE based

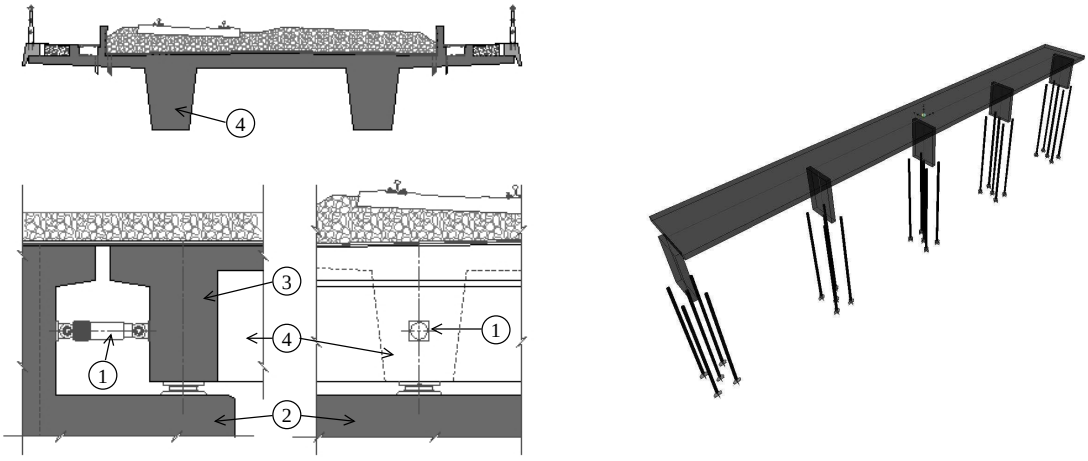

Legend: 1. SMA device, 2. Abutment, 3. Transverse girder, 4. Main girder

Figure 4. São Martinho railway viaduct: Mid-span cross section, SMA passive control device location and finite element model.

passive seismic control device for the longitudinal analysis of the segment. The analysis is made assimilating it with a SDOF dynamic system with 4650 ton mass and stiffness of 355×10^3 kN/m. Pre-strained NiTi SE restraining elements ($\varepsilon_0 = 3.5\%$) are placed at the ends of the viaduct, one for each main girder, working in combination with the bearings. In order to clarify the effect of the SE elements in the dynamic behaviour of the structure, a parametric study considering a variation of the total SE restraining area up to an arbitrary value of $A_{max} = 950$ cm^2 is made. The structure of the viaduct is considered to behave elastically.

The seismic action is introduced in the system by means of artificially generated accelerograms using the design acceleration power spectral density functions. Given the random nature of these generated accelerograms, the viaduct is submitted to six different series, represented in Figure 5.

During the seismic events, if the minimum stress to induce the martensitic transformation in the SE elements is not attained, they behave like additional linear elastic materials, increasing the system's stiffness. The displacement amplitude of the structure is hence decreased, but at the cost of increasing the system's natural frequency and leading to an undesirable increase in structural accelerations [19]. The

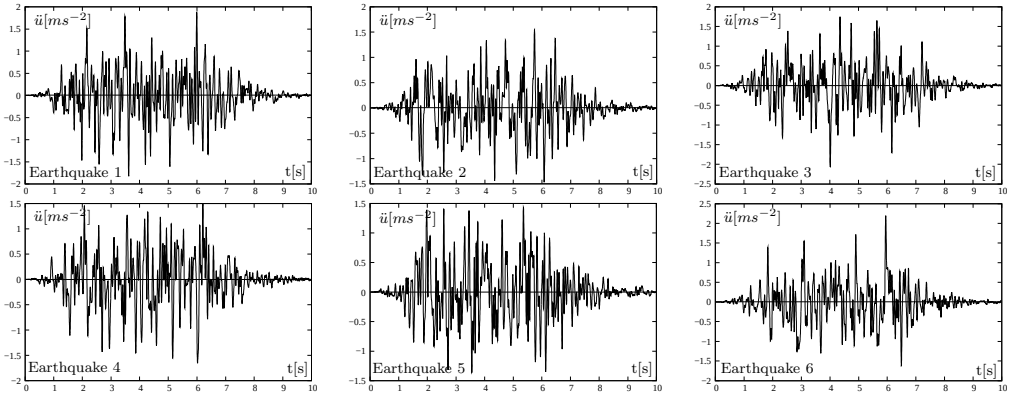

Figure 5. Generated accelerograms.

introduction of a pre-strain in the SE elements facilitates the beginning of the martensitic transformation and the corresponding hysteretical energy dissipation.

With illustrative purpose, the seismic responses of the viaduct for a restraining area of 40 cm^2 (5% A_{max}), in what respect the longitudinal displacement, velocity and acceleration time-histories and the corresponding force-displacement diagram in the SE restraining elements, is presented in Figure 6 for earthquake 1.

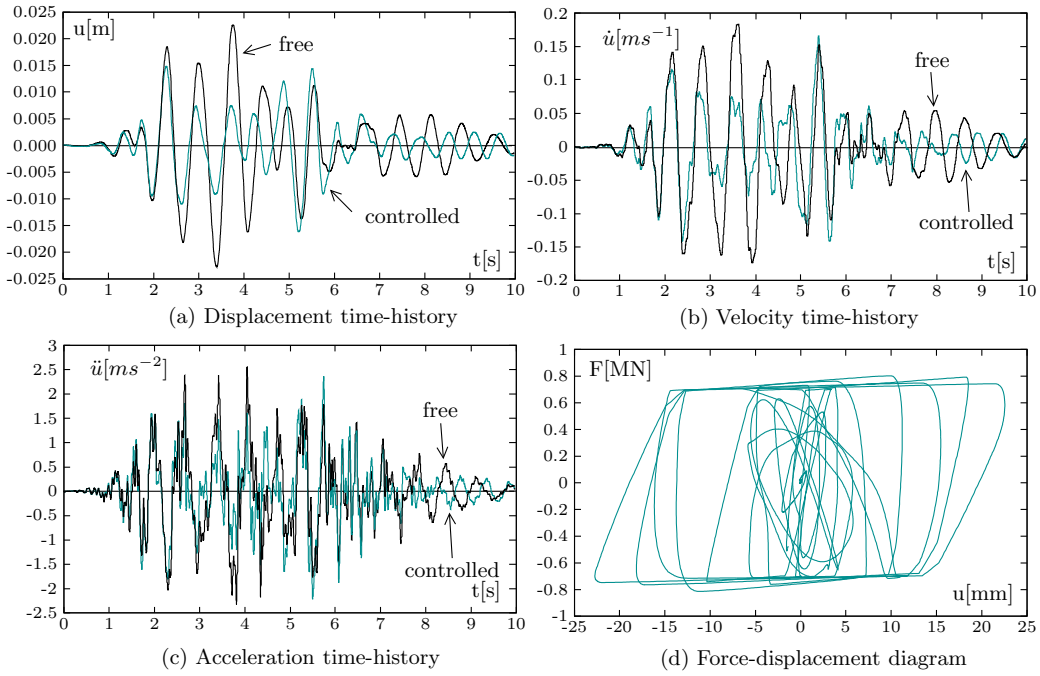

Figure 6. Seismic response of the viaduct for a restraining area of 5% A_{max}.

One can see that there is an important reduction of the amplitude of the longitudinal displacement of the viaduct, as well as of the corresponding velocity and acceleration. Due to the presence of a loading plateau in the SE hysteresis, related to the forward

martensitic transformation, the total SE force in the restraining elements is conveniently bounded, limiting the force which is transmitted to the structure during the seismic event.

The influence of the area of the SE restraining elements in the seismic response of the viaduct is translated in the curves presented in Figure 7, obtained using the average value of the maximum response resulting from the set of six accelerograms. According to

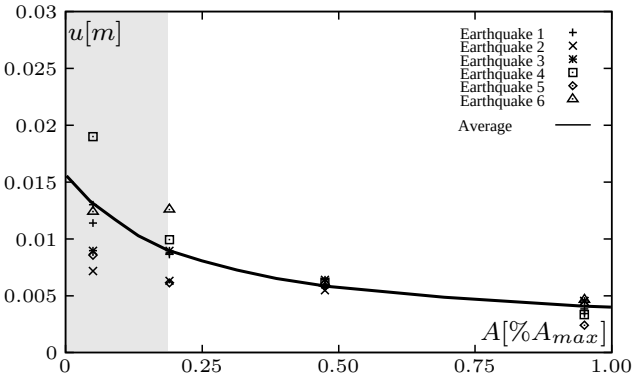

(a) Longitudinal displacement

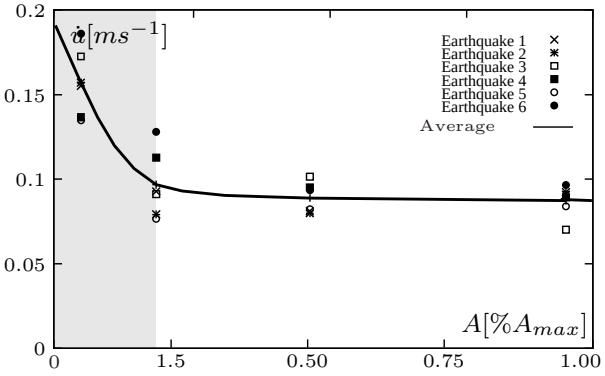

(b) Longitudinal velocity

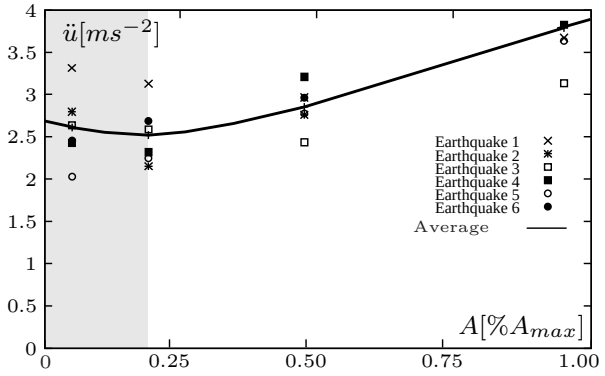

(c) Longitudinal acceleration

Figure 7. Longitudinal displacement, velocity and acceleration of the deck in function of the SE restraining area.

the obtained results, one can see that for increasing areas of the SE restraining elements the mean longitudinal displacement and velocity of the deck decrease monotonously. In what concerns the mean longitudinal acceleration of the deck, it's value tends to decrease until it reaches a minimum threshold, which corresponds to about 20% of the maximum SE restraining area, before starting to increase once more. The shaded regions of the graphs represent the most effective SE restraining solutions for the passive control of the viaduct, where it's seismic response in terms of displacements and velocity suffers the most important reduction, up to 40 and 50%, respectively, and the acceleration decreases, up to 10%. Therefore, one can say that with a SE restraining area of 20% of the maximum considered area one obtains an optimised solution for the seismic passive mitigation. If one increases the SE restraining area, one can further reduce the seismic response in terms of displacements and velocities, but at the cost of increasing the acceleration values. Regarding the acceleration time-history, one can say that, for a given seismic action, as long as the total area of the SE restraining elements enables a considerable extent of the martensitic transformation, the dissipation capacity of the system increases with the SE restraining area, decreasing the longitudinal acceleration of the deck. Above a certain threshold, as the stiffness of the SE restraining elements continues to increase, the extent of the martensitic transformation starts to decrease, the acceleration increases and the natural frequency of the viaduct is shifted to higher values.

5. Conclusions

This paper studies the retrofitting of a viaduct in order to modify it's seismic response in terms of longitudinal deck displacement, velocity and acceleration, while preventing span unseating. The retrofitting solution is based on the use of SE SMA seismic links, featuring high dissipation and high re-centering capabilities. The analysis is based on the numeric simulation of the viaduct's longitudinal behavior, together with SE restoring elements, when subjected to a series of artificially generated accelerograms. The constitutive model describing the complex SE thermo-mechanical behavior of the seismic links is also presented and validated. In order to enhance the dissipation capacity of the SE restraining solution, two pre-strained restoring elements are used, working in phase opposition, which yield an equivalent viscous damping of about 23%. A parametric study concerning the SE area of the restraining system allows to identify the optimal compromise between the cross-sectional area of the SE restraining elements and the seismic mitigation capacity of the system regarding the longitudinal deck displacement, velocity and acceleration. For the case studied, this optimal SE restraining window, where the longitudinal displacement and velocity of the system are significantly reduced, together with a reduction of the corresponding acceleration field, is bounded by a SE restraining area of about 190 cm^2.

Acknowledgments

This work is part of the research developed in the Department of Civil Engineering, Faculdade de Ciências e Tecnologia, supported by contract SFRH/BD/37653/2007 with Fundação para a Ciência e Tecnologia.

References

[1] CEN. *Eurocode 8 - Design of structures for earthquake resistance - Part 2: Bridges. Ref. No. EN 1998-2:2005: E*, 2005.

[2] J. E. Padgett, R. DesRoches, and R. Ehlinger. Experimental response modification of a four-span bridge retrofit with shape memory alloys. *Structural Control and Health Monitoring*, 2009.

[3] R. DesRoches. Application of shape memory alloys in seismic rehabilitation of bridges. Technical Report NCHRP-91, IDEA Program, Transportation Research Board, National Research Council, 2005.

[4] R. Johnson, J. E. Padgett, M. E. Maragakis, R. DesRoches, and M. S. Saiidi. Large scale testing of Nitinol shape-memory alloy devices for retrofitting of bridges. *Smart Materials and Structures*, 17(3), 2008.

[5] B. Andrawes and R. DesRoches. Comparison Between Shape Memory Alloy Restrainers and and Other Bridge Retrofit Devices. *ASCE Journal of Bridge Engineering*, 12(6):700–709, 2007.

[6] R. DesRoches and M. Delemont. Seismic retrofit of simply supported bridges using shape memory alloys. *Engineering Structures*, 24:325–332, 2002.

[7] R. DesRoches, T. Pfeifer, R. T. Leon, and T. Lam. Full-Scale Tests of Seismic Cable Restrainer Retro?ts for Simply Supported Bridges. *Journal of Bridge Engineering*, 8(4):191–198, 2003.

[8] L. C. Brinson and M. S. Huang. Simplifications and Comparisons of Shape Memory Alloy Constitutive Models. *Journal of Intelligent Material Systems and Structures*, 7:108–114, 1996.

[9] C. Liang and C. A. Rogers. One-Dimensional Thermomechanical Constitutive Relations for Shape-Memory Materials. *Journal of Intelligent Systems and Structures*, 1:207–234, 1990.

[10] S. De la Flor and F. F. Urbina. Constitutive model of shape memory alloys: Theoretical formulation and experimental validation. *Materials Science and Engineering A*, 427(1-2):112–122, 2006.

[11] C. L. Magee. Nucleation of martensite. In ASM, editor, *Phase Transformations*, pages 115–156. 1970.

[12] A. Vitiello, G. Giorleo, and R. E. Morace. Analysis of thermomechanical behaviour of Nitinol wires with high strain rates. *Smart Materials and Structures*, 14:215–221, 2005.

[13] K. Tanaka, S. Kobayashi, and Y. Sato. Thermomechanics of transformation pseudoelasticity and shape memory effect in alloys. *International Journal of Plasticity*, 2:59–72, 1986.

[14] K. Tanaka, F. Nishimura, T. Hayashi, H. Tobushi, and C. Lexcellent. Phenomenological analysis on subloops and cyclic behavior in shape memory alloys under mechanical and/or thermal loads. *Mechanics of Materials*, 19:281–292, 1995.

[15] F. P. Incropera and D. P. DeWitt. *Fundamentals of heat and mass transfer*. John Wiley and Sons, Inc., 6th edition, 2006.

[16] C. Cismasiu and F. P. A Santos. Numerical simulation of superelastic shape memory alloys subjected to dynamic loads. *Smart Materials and Structures*, 17(2):25–36, 2008.

[17] M. Dolce, D. Cardone, and R. Marnetto. Implementation and testing of passive control devices based on shape memory alloys. *Earthquake Engineering and Structural Dynamics*, (29):945–968, 2000.

[18] Y. Zhang and S. Zu. A shape memory alloy-based reusable hysteretic damper for seismic hazard mitigation. *Smart Materials and Structures*, 16:1603–1623, 2007.

[19] S. Seelecke, O. Heintze, and A. Masuda. Simulation of earthquake-induced structural vibrations in systems with SMA damping elements. *SPIE Smart Structures and Materials*, 4697, 2002.